A modified interval subdividing based geometric calibration method for interior tomography*

Zhang Feng(张 峰), Yan Bin(闫 镔)†, Li Lei(李 磊),
Xi Xiao-Qi(席晓琦), and Jiang Hua(江 桦)

National Digital Switching System Engineering & Technology Research Center, Zhengzhou 450002, *China*

(Received 20 October 2013; revised manuscript received 23 December 2013; published online 16 July 2014)

The interior tomography is commonly met in practice, whereas the self-calibration method for geometric parameters remains far from explored. To determine the geometry of interior tomography, a modified interval subdividing based method, which was originally developed by Tan *et al.*,[11] was presented in this paper. For the self-calibration method, it is necessary to obtain the reconstructed image with only geometric artifacts. Therefore, truncation artifacts reduction is a key problem for the self-calibration method of an interior tomography. In the method, an interior reconstruction algorithm instead of the Feldkamp–Davis–Kress (FDK) algorithm was employed for truncation artifact reduction. Moreover, the concept of a minimum interval was defined as the stop criterion of subdividing to ensure the geometric parameters are determined nicely. The results of numerical simulation demonstrated that our method could provide a solution to the self-calibration for interior tomography while the original interval subdividing based method could not. Furthermore, real data experiment results showed that our method could significantly suppress geometric artifacts and obtain high quality images for interior tomography with less imaging cost and faster speed compared with the traditional geometric calibration method with a dedicated calibration phantom.

Keywords: interior tomography, geometric calibration, interval subdividing, minimum interval

PACS: 87.59.–e, 87.59.bd **DOI:** 10.1088/1674-1056/23/9/098704

1. Introduction

The global cone-beam computed tomography (CT) is widely utilized in various research fields, which requires that the scanned object is completely covered by the field of view (FOV). In practice, however, region of interest (ROI) tomography may be more desirable in some circumstances due to the features of low radiation dose and fast imaging speed. Especially, the cases where the ROIs exist in the interior of the object, called interior tomography, are commonly met. For all applications of cone-beam CT, the reconstructed image quality depends highly on the precise geometry of the system. Consequently, geometric calibration is necessary for either global tomography or interior tomography.

Significant progress has been made in the field of geometric calibration for global tomography.[1–10] Some directly utilized the projections of scanned objects[6–10] to determine the geometric parameters without dedicated phantoms, referred to as self-calibration. The self-calibration methods are more attractive in practice. In these methods, Brunette *et al.*[6] estimated the geometric parameters by minimizing the object area in the reconstructed image. Based on the sinogram, two methods were researched by Panetta *et al.*[7] and Patel *et al.*,[8] respectively. Since the entropy of the reconstructed image was influenced by geometric artifacts, the geometric parameters were determined by entropy minimization in Ref. [9]. Subsequently, Kingston *et al.* proposed a method based on the sharpness of reconstructed image maximization to obtain the sharpest three-dimensional (3D) reconstruction.[10] Very recently, a practical and robust method based on interval subdividing was researched by Tan *et al.*[11] As is well known, reconstruction of an image with only the geometric artifacts is necessary for all self-calibration methods. Thus, self-calibration for interior tomography is more difficult than that for global tomography because of the presence of projection data truncation artifacts.

As far as we know, no self-calibration method for interior tomography has been reported. Although the Tan *et al.* method is fast and robust, it cannot be applied in interior tomography directly because of its sensitivity to the truncation artifacts. Based on the Tan *et al.* method, a modified geometric calibration method for interior tomography was proposed in this paper. In this method, an interior reconstruction algorithm instead of the FDK algorithm[12] in the original method was employed to reduce the truncation artifacts. Moreover, the concept of minimum interval was defined and considered to be the stop criterion of subdividing to ensure the geometric parameters are determined nicely. To verify the feasibility and efficiency of our method, a numerical simulation and a real-data experiment were implemented.

The remainder of the paper is organized as follows. The

*Project supported by the National Basic Research Program of China (Grant No. 2011CB707701), the National High Technology Research and Development Program of China (Grant No. 2012AA011603), and the National Natural Science Foundation of China (Grant Nos. 30970772 and 61372172).

†Corresponding author. E-mail: tom.yan@gmail.com

© 2014 Chinese Physical Society and IOP Publishing Ltd

geometry of cone-beam CT is described in Section 2. The theory of our method is introduced in detail in Section 3. Section 4 discusses the results of simulation and real-data experiment. Finally, conclusions are summarized in Section 5.

2. Geometry description of interior tomography

2.1. Cone-beam projection and image reconstruction

The cone-beam projection denoted by $\boldsymbol{g}$ can be expressed as

$$\boldsymbol{g} = \boldsymbol{A}_{\boldsymbol{\lambda}} \boldsymbol{f}, \tag{1}$$

where $\boldsymbol{A}_{\boldsymbol{\lambda}}$ is the linear integral operator, $\boldsymbol{\lambda}$ is the vector of geometric parameters, and $\boldsymbol{f}$ is the density function of the object. When the complete projections are available, the image reconstruction can be written as

$$\boldsymbol{f} = (\boldsymbol{A}_{\boldsymbol{\lambda}})^{+} \boldsymbol{g}, \tag{2}$$

where $(\boldsymbol{A}_{\boldsymbol{\lambda}})^{+}$ is the inverse of $\boldsymbol{A}_{\boldsymbol{\lambda}}$. In the two-dimensional (2D) parallel-beam CT, $\boldsymbol{A}_{\boldsymbol{\lambda}}$ is the Radon transform, and $(\boldsymbol{A}_{\boldsymbol{\lambda}})^{+}$ is the inverse Radon transform. If the geometric parameters are misaligned, denoted by $\boldsymbol{\lambda}^{*}$, the corresponding acquired set of projections are denoted by $\boldsymbol{g}^{*}$. By applying Eq. (2), the reconstructed image is $\boldsymbol{f}^{*} = (\boldsymbol{A}_{\boldsymbol{\lambda}})^{+} \boldsymbol{g}^{*}$. Obviously, the resulting reconstructed image $\boldsymbol{f}^{*}$ is interfered by geometric artifacts because $\boldsymbol{f}^{*} \neq \boldsymbol{f}$. To obtain a high quality tomographic image, we have to determine the misaligned set of geometric parameters $\boldsymbol{\lambda}^{*}$. Technically speaking, different geometric parameters need to be determined in different scan orbits. In this paper, we mainly discuss the geometric calibration method in circular cone-beam CT.

2.2. Geometric parameters in circular cone-beam CT

The geometry of circular cone-beam CT is shown in Fig. 1. The x axis points to the X-ray source, the z axis is along the rotation axis, and the y axis is perpendicular to the x–z plane. In the geometry, the geometric parameters to be determined are described as follows.

(i) D, the distance from the X-ray source to the detector.

(ii) (u_0, v_0), coordinates of the orthogonal projection of the X-ray focal spot onto the detector.

(iii) R, the distance from the X-ray source to the rotation axis.

(iv) η, the rotation angle of the detector about normal vector $\boldsymbol{e}_w$.

(v) ϕ, the rotation angle of the detector about the $u = u_0$ axis.

(vi) θ, the rotation angle of the detector about the $v = v_0$ axis.

Interior tomography means that the acquired projections are truncated on both lateral sides. The geometric parameters of interior tomography can be collected into vector $\boldsymbol{\lambda}_{\mathrm{c}} = (D, u_0, v_0, R, \eta, \phi, \theta)^{\mathrm{T}}$. Considering that parameter D is constant after the CT system is manufactured and R only affects the systematic magnification, which is unrelated to the reconstructed image quality, only the remaining five parameters are taken into account. Among the five parameters, von Smekal *et al.*[2] and Yang *et al.*[4] have demonstrated that the transversal shift u_0 and skew of detector η are critical for the image quality. Therefore, ϕ and θ are assumed to be zero, R is measured approximately, and v_0 is considered as the center of the detector in the latitude direction. As a result, only geometric parameters u_0 and η collected into vector $\lambda_{\mathrm{c}} = (u_0, \eta)^{\mathrm{T}}$ are calibrated in this paper.

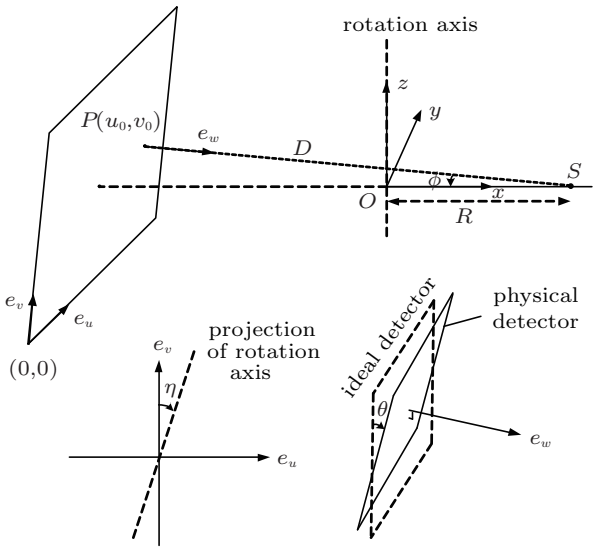


Fig. 1. Geometry of the circular cone-beam CT.

3. Theory

3.1. The original interval subdividing based method

The original method proposed by Tan *et al.* is practical for global tomography. The main idea of the method is to equally divide the interval of the geometric parameter into small parts and analyze the quality between every two reconstructed slices on each end point of one part. Let $I_a(x,y,n)$ and $I_b(x,y,n)$ be the two slices, of which a and b are the end points of one part. The value of Q is defined as the similarity of the two slices and calculated by

$$Q(a,b,n) = 1 - \frac{\sum\limits_{(x,y)\in \boldsymbol{M}} [I_a(x,y,n) - I_b(x,y,n)]^2}{N \times p^2}, \tag{3}$$

where (x,y) are the coordinates of pixel, $\boldsymbol{M}$ is the slice matrix, N is the number of pixels in each slice, and n is the slice index in the reconstructed volume. According to the definition of Q, we know that it will increase with the increase of the similarity of $I_a(x,y,n)$ and $I_b(x,y,n)$. When $I_a(x,y,n)$ is the same as $I_b(x,y,n)$, i.e., $a = b$, Q is equivalent to one. To ensure that $Q(a,b,n)$ is between 0 and 1, p is equivalent to the maximum

value of a pixel in one slice. For every interval subdivision, the interval corresponding to the maximum value of Q is found and set to be the next waiting subdivided interval. It is noticed that the interval may need to be expanded to ensure the trend line is nonlinear for the first subdivision. For each geometric parameter, the processes of subdividing are repeated until the resultant interval is narrowed to less than sub-pixel.

3.2. The proposed method

In the interior tomography, reconstructed images are always degraded by truncation artifacts. However, the influence of truncation artifacts to the Q value was not considered in the original interval subdividing method. Thus, truncation artifacts reduction is the first consideration for interior tomography.

3.2.1. Truncation artifacts reduction

It is well known that reconstruction of an image with only geometric artifacts is necessary for the self-calibration method. In the original calibration method, the reconstructed slices are obtained by using the FDK algorithm. If the original method is employed to deal with the truncated projections acquired in interior tomography, the non-local characteristics of the FDK algorithm will produce severe truncation artifacts in the reconstructed image. The truncation artifacts are seen in the form of bright cupping artifacts at the edges, and a difference in CT numbers compared with global reconstructions.[14] In the two types of artifacts, the calculation of the Q value is mainly interfered with by the bright cupping artifacts. Therefore, reduction of the cupping artifacts is a key problem for self-calibration of interior tomography. To avoid complicated computations, the FDK algorithm of the original method is replaced by an approximate interior reconstruction algorithm.

The present interior reconstruction algorithms can be divided into exact and approximate ones. Although the exact algorithms can reconstruct images exactly, it is computationally extensive.[14–16] Compared with the exact algorithms, the approximate algorithms are efficiently computational and can reduce the cupping artifacts at the edges. As stated in the previous paragraph, reduction of cupping artifacts is beneficial to the calculation of the Q value. The approximate truncation robust computed tomography (ATRACT) algorithm firstly proposed by Dennerlein *et al.* was one of the most efficient approximate algorithms.[17–20] The ATRACT-type algorithm can significantly reduce truncation artifacts with the idea of "local filtering plus global filtering" instead of the ramp filtering in the FDK algorithm. To improve the computation efficiency, a new method was proposed by Wang *et al.*[21], which can be described as follows.

Step 1 Weighting the projection data

$$g_1(\lambda,u,v)=\frac{D}{\sqrt{D^2+u^2+v^2}}g(\lambda,u,v), \tag{4}$$

where D is the distance from the X-ray source to the detector, $g(\lambda,u,v)$ is the projection at view of λ, and (u,v) are coordinates of the detector pixel.

Step 2 First-order derivation of the weighted projection with respect to u

$$g_2(\lambda,u,v)=\frac{\partial}{\partial u}g_1(\lambda,u,v). \tag{5}$$

Step 3 Hilbert filtering of $g_2(\lambda,u,v)$

$$g_3(\lambda,u,v)=\frac{1}{2\pi}g_2(\lambda,u,v)\otimes h_{\mathrm{H}}(u), \tag{6}$$

where $h_{\mathrm{H}}(u)=1/(\pi u)$ is the Hilbert transform kernel, and the symbol $\otimes$ represents convolution.

Step 4 Back-projecting the filtered projections onto the 3D image

$$f(\boldsymbol{r})=\frac{1}{2}\int_0^{2\pi}\frac{RD}{\left[R-\boldsymbol{r}\cdot\boldsymbol{n}_w(\lambda)\right]^2}g_3(\lambda,u^*,v^*)\,\mathrm{d}\lambda, \tag{7}$$

where R is the distance from the X-ray source to the rotation axis, $\boldsymbol{n}_w(\lambda)$ is the unit vector from the X-ray source to the detector, (u^*,v^*) are projected coordinates of one voxel point $\boldsymbol{r}=(x,y,z)^{\mathrm{T}}$ which can be calculated by

$$u^*=\frac{Dy}{R-\boldsymbol{r}\cdot\boldsymbol{n}_w(\lambda)},\quad v^*=\frac{Dz}{R-\boldsymbol{r}\cdot\boldsymbol{n}_w(\lambda)}. \tag{8}$$

3.2.2. The stop criterion of subdividing

In the original method, the stop criterion of subdividing was not discussed carefully in theory. Here, the concept of a minimum interval which is defined by the perturbation in the parameter value causing the appearance of geometric artifacts is introduced. If the waiting subdivided interval was narrowed to less than the minimum interval, the process of subdividing will be stopped. In the paper, the minimum interval of u_0 is defined as 1 pixel width and that of η is defined as $\arctan(1/H)$ radian where H is the height of the detector in unit of pixel.

In our method, the calibration order is that the parameter u_0 is calibrated firstly, followed by the calibration of the parameter η. The slices from the midplane, i.e., $z=0$, are chosen to estimate the Q value in the calibration process of parameter u_0. When the minimum interval of u_0 is reached, the resulting u_0 is determined by

$$u_0=\frac{u_0^a+u_0^b}{2}, \tag{9}$$

where u_0^a and u_0^b are the values of end points of the last interval. Then, the parameter η is calibrated with the fixed u_0. In the calibration process of parameter η, the slices that are close to the top of the reconstructed image are chosen in the Tan *et al.* method. However, the slices that are close to the top of reconstructed image may be influenced by cone angle artifacts. To reduce the interference of cone angle artifacts, the

slices from the vertical plane at $x = 0$ or $y = 0$ are chosen in our method. When the minimum interval $[\eta^a, \eta^b]$ is reached, the calibration result is calculated by

$$\eta = \frac{\eta^a + \eta^b}{2}. \tag{10}$$

4. Experimental results

To verify the efficiency of the proposed method, a numerical simulation and a real data experiment were implemented. In the simulation, both the Tan *et al.* method and our method were implemented to demonstrate the capability of our method in the geometric calibration of interior tomography. To show the advantages of imaging cost reduction and fast speed of the proposed method compared with the traditional geometric calibration method, the Noo *et al.* method[1] was also implemented in the real data experiment. The Noo *et al.* method is a classical geometric calibration method for circular scan. It uses the parameters of two ellipses that are the projected images of two circles, which are the orbits of two steel balls positioned in a dedicated phantom, to determine the geometry.

4.1. Numerical simulation

In the simulation, the truncated projections of the 3D Shepp–Logan phantom[22] were simulated with a circular trajectory. The size of the phantom was 51.2 mm×51.2 mm×51.2 mm, of which the central circle area with a radius of 10 mm was selected as the interior ROI. The measured projections only contain the linear integrals of rays passing through the ROI and the parameters of the numerical simulation are shown in Table 1.

Table 1. Parameters of the numerical simulation.

Parameters	Value
Source to object distance	300 mm
Source to detector distance	600 mm
Size of detector	256 pixel×256 pixel
Size of detector cell	0.2 mm×0.2 mm
Number of projections in 2π	360
u_0	27.5 mm
η	1.2 degrees

The parameter u_0 was calibrated firstly with the slices at the midplane, of which the reconstruction matrix was set to be 256×256 with a pixel size 0.1 mm×0.1 mm. The number of reconstructions in every subdividing was 3 and the initial interval of u_0 was [22 mm, 34 mm]. In the calibration process of parameter u_0, η was set to be 0. In the first subdividing, the subintervals were [22, 26], [26, 30], and [30, 34]. The values of Q calculated using the Tan *et al.* method are shown in Fig. 2 and the reconstructed images corresponding to the four end points are shown in Fig. 3. In Fig. 3, it is found that the images are polluted by truncation artifacts and the Q values are mainly determined by truncation artifacts instead of the density function of the object. As a result, the search direction shown in Fig. 2 is incorrect.

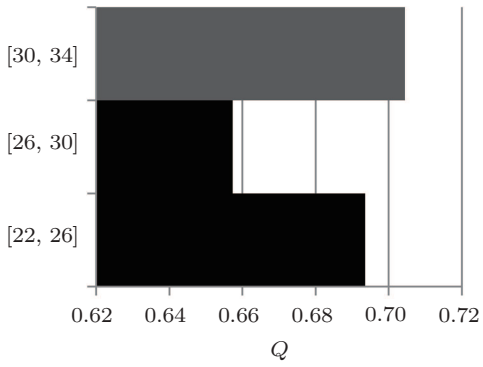


Fig. 2. The subdividing for the interval and the corresponding Q values.

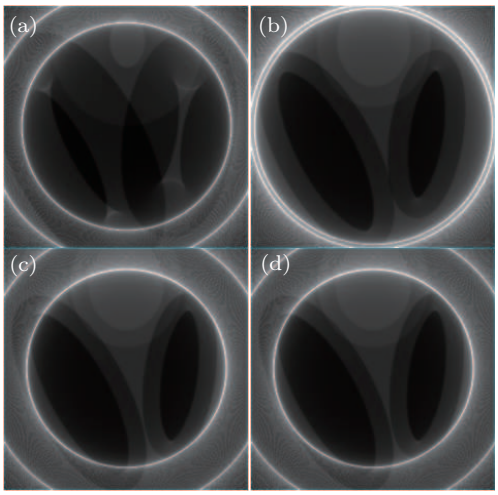


Fig. 3. The reconstructed images of the midplane corresponding to the four end points. The display window is [0,3]. (a) $u_0 = 22$ mm, (b) $u_0 = 26$ mm, (c) $u_0 = 30$ mm, (d) $u_0 = 34$ mm.

To reduce the truncation artifacts, the FDK algorithm in the original method is replaced by the Wang *et al.* method in our method. The subdividing for the interval and change of Q values are shown in Fig. 4. From which, we can find that the stop criterion of parameter u_0 is reached and the resulting interval is [27.5, 27.6] after subdividing four times. Thus, the calibration result of parameter u_0 is 27.55 mm according to Eq. (9). The four reconstructed images of the last subdividing are shown in Fig. 5. It is noticed that the p of Eq. (3) should be calculated by $\max\{|I_a(x,y,n)) - I_b(x,y,n)|\}$ since the pixel value of the reconstructed image may be negative caused by the Wang *et al.* method.

The initial interval of parameter η was $[-2^\circ, 2^\circ]$ and the number of reconstructions in every subdividing was three. The slices at $x = 0$ were chosen to calibrate the parameter η. The calibration processes of parameter η were repeated with the parameter $u_0 = 27.55$ mm, and the results are shown in Fig. 6.

After subdividing three times, the minimum interval of parameter η was reached and the calibration result was 1.335° according to Eq. (10). The reconstructed images of the last subdividing are shown in Fig. 7. The simulation results demonstrate that the measuring errors of parameters u_0 and η are less than the minimum intervals by using our method.

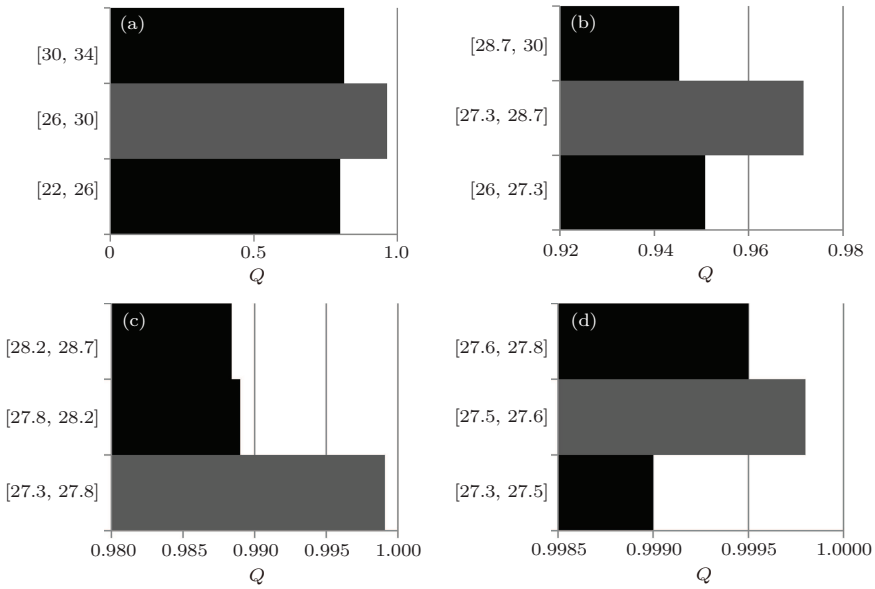


Fig. 4. The subdividing of transversal shift in numerical simulations. (a) Q values of the first subdividing, (b) the second subdividing, (c) the third subdividing, and (d) the last subdividing.

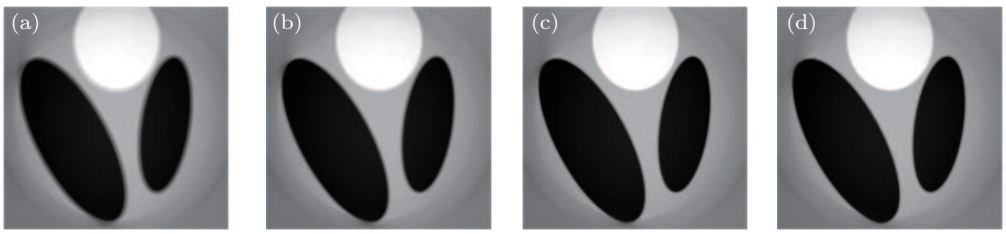


Fig. 5. The reconstructed images of the last subdividing. The display window is $[-1, 1]$. (a) $u_0 = 27.3$ mm, (b) $u_0 = 27.5$ mm, (c) $u_0 = 27.6$ mm, (d) $u_0 = 27.8$ mm.

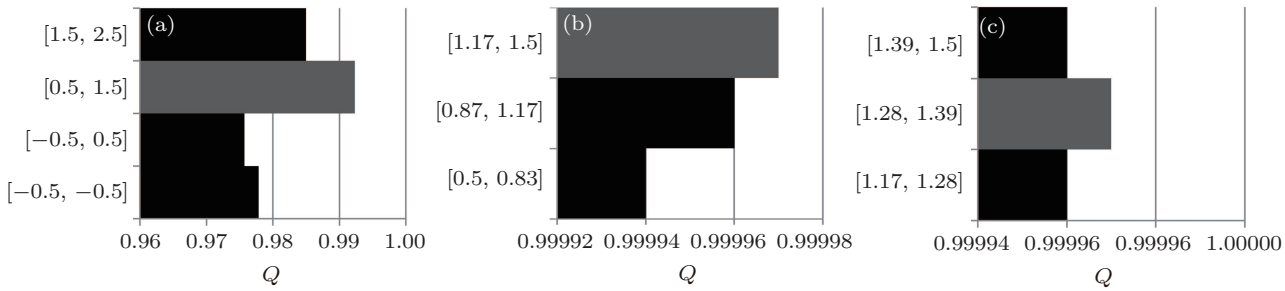


Fig. 6. The subdividing of the detector skew in numerical simulation. (a) Q values of the first subdividing, (b) the second subdividing, and (c) the last subdividing.

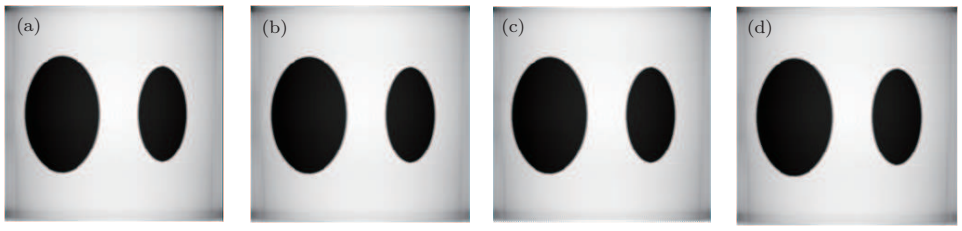


Fig. 7. The reconstructed images of the last subdividing. The display window is $[-1, 1]$. (a) $\eta = 1.17°$, (b) $\eta = 1.28°$, (c) $\eta = 1.39°$, (d) $\eta = 1.5°$.

4.2. Real data experiment

To verify the capability of our method in dealing with real data, an experiment was implemented on our laboratory CT. In the experiment, 360 projections (2304×3200 pixels) with the resolution of 0.127 mm/pixel of the printed circuit board (PCB) were acquired in a full circular scan. The distances from the source to the object and the detector were 503 mm and 1435 mm, respectively. The voxel size of the reconstructed volume was 0.045 mm. To obtain the truncated projections, the central 512×512 pixels of all projections were cropped virtually. Like the numerical simulation, the calibration processes of the parameters u_0 and η are shown in Figs. 8 and 9, respectively. Finally, the calibration results are $u_0 = 29.63$ mm and $\eta = 0.335°$. With the calibrated geometric parameters, the corrected reconstructed image is obtained and shown in Fig. 10(b).

Additionally, the Noo *et al.* method[1] was also implemented. According to the Noo *et al.* theory, 60 projections of the dedicated calibration phantom were additionally acquired to determine the geometric parameters, and then, the complete projections were corrected with the geometric parameters and the global reconstruction of PCB was obtained by using the FDK algorithm. The ROI of the global reconstructed image corresponding to the reconstructed image from the above cropped projections is shown in Fig. 10(c).

The reconstructed image without geometric calibration is shown in Fig. 10(a). The uncorrected image is severely degraded by geometric artifacts, e.g., the wires in Fig. 10(a) are blurred. Compared with the uncorrected image, the geometric artifacts of calibrated images using our method and the Noo *et al.* method are significantly restrained. For example, the wires in Figs. 10(b) and 10(c) are sharp. In contrast to the reconstructed image using the Noo *et al.* method, it can be found that our method can provide considerable image quality. However, the Noo *et al.* method will shorten

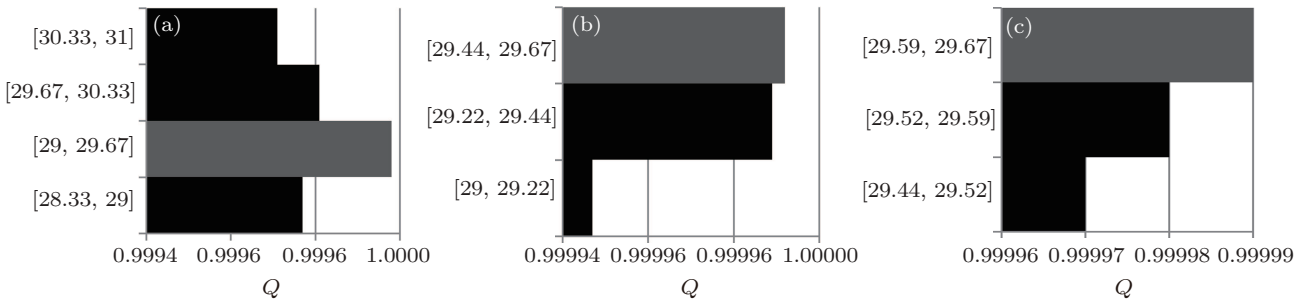


Fig. 8. The subdivision of transversal shift in the real data experiment. (a) Q values of the first subdivision, (b) the second subdivision, and (c) the last subdivision.

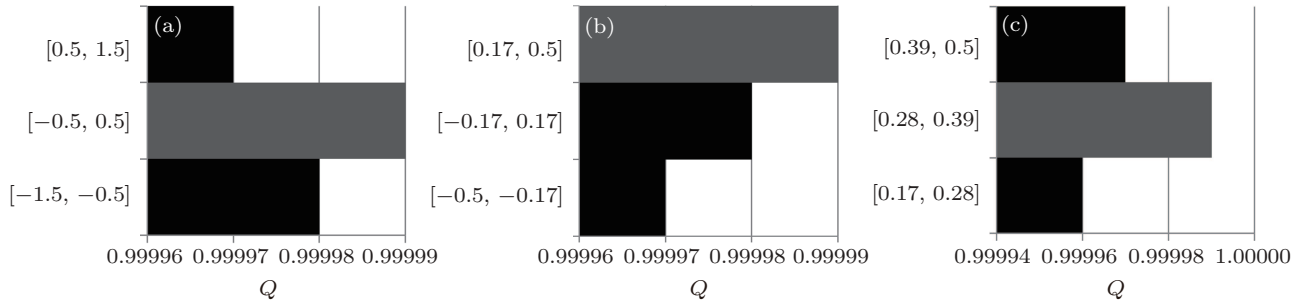


Fig. 9. The subdivision of skew of the detector in the real data experiment. (a) Q values of the first subdivision, (b) the second subdivision, and (c) the last subdivision.

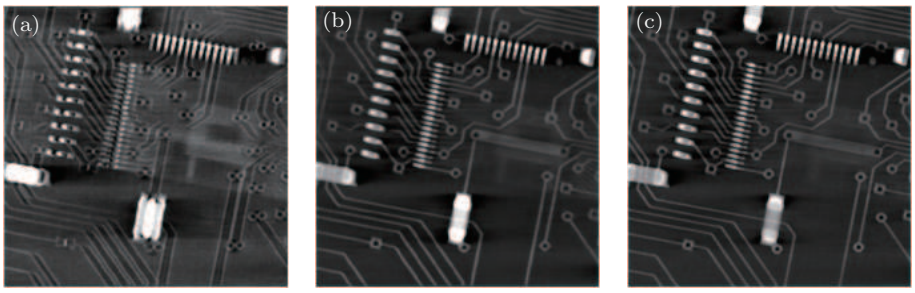


Fig. 10. The image without geometric calibration (a), the calibrated image using our method from virtually cropped projections (b), and the corrected image using the Noo *et al.* method (c). The display window is [−1, 5].

the lifetimes of hardware and increase the imaging cost because additional projection acquisitions of the calibration phantom are needed. In contrast, our method has the advantage of imaging cost reduction. Moreover, geometric parameter calculations from projections of the dedicated phantom are included in the Noo *et al.* method while our method directly determines the geometry from the raw projections. In the experiment, the calculation time of the Noo *et al.* method and our method is approximately 3 min and 0.5 min, respectively. Therefore, the proposed method has the advantage of faster speed.

5. Conclusion

In this paper, a modified interval subdivision based on the geometric method for interior tomography was proposed. To reduce the truncation artifacts, an interior reconstruction algorithm instead of the FDK algorithm in the original method was employed in our method. Moreover, the stop criterion of subdivision based on the concept of a minimum interval was defined to insure the geometric parameters are determined nicely. The results of the numerical simulation demonstrated that our method was efficient for the interior tomography while the original methods did not work. Furthermore, real-data experiment results showed that our method can significantly suppress geometric artifacts and obtain high-quality images for interior tomography with less imaging cost and faster speed compared with the traditional geometric calibration methods.

In practice, the proposed method may have two potential limitations. The first limitation is that the cost function of geometric artifacts may need to be changed in different applications. In other words, the Q value is sensitive to high contrast objects (e.g., industrial parts) but insensitive to low contrast ones (e.g. soft tissues of the human body). The second one is that the initial interval of each geometric parameter should include the real value and the length of which should be as narrow as possible for fast geometric calibration.

References

[1] Noo F, Clackdoyle R, Mennessier C, White T A and Roney T J 2000 *Phys. Med. Biol.* **45** 3489

[2] Smekal V L, Kachelriess M, Stepina E and Kalender W A 2004 *Med. Phys.* **31** 3242

[3] ChoY, Moseley D J and Siewerdsen J H 2005 *Med. Phys.* **32** 968

[4] Yang K, Kwan A L C, Miller D F and Boone J M 2006 *Med. Phys.* **33** 1695

[5] Wu D F, Li L, Zhang L and Xing Y X 2011 *Nuclear Science Symposium and Medical Imaging Conference (NSS/MIC)*, October 23–29, 2011 Valencia, Spain, p. 2952

[6] Brunetti A and Carlo F D 2004 *Developments in X-Ray Tomography IV*, October 2–6, 2004 Colorado, USA, p. 652

[7] Panetta D, Belcari N and Guerra A D 2008 *Phys. Med. Biol.* **53** 3841

[8] Patel V, Chityala R N, Hoffman K R, Ionita C N, Bednarek D R and Rudin S 2009 *Med. Phys.* **36** 48

[9] Kyriakou Y, Lapp R and Hillebrand L 2008 *Phys. Med. Biol.* **53** 6267

[10] Kingston A Sakellariou A, Varslot T, Myers G and Sheppard A 2011 *Med. Phys.* **38** 4934

[11] Tan S Q, Cong P, Liu X M and Wu Z F 2013 *NDT&E Int.* **58** 49

[12] Feldkamp L, Davis L C and Kress J W 1984 *J. Opt. Soc. Am. A* **1** 612

[13] Sharma K S, Holzner C, Vasilescu D M, Jin X, Narayanan S, Agah M, Hoffman E A, Yu H Y and Wang G 2013 *Phys. Med. Biol.* **58** 4297

[14] Yu H Y and Wang G 2009 *Phys. Med. Biol.* **54** 2791

[15] Yang J S, Yu H Y, Jiang M and Wang G 2010 *Inverse Probl.* **26** 35013

[16] Jin X, Katsevich A, Yu H Y, Wang G, Li L and Chen Z Q 2012 *IEEE Trans. Med. Imaging* **31** 2108

[17] Dennerlein F 2011 11*th International Meeting on Fully Three-dimensional Image Reconstruction in Radiology and Nuclear Medicine*, July 11–15, 2011 Potsdam, Germany, p. 80

[18] Xia Y, Maier A, Dennerlein F, Hofmann H G and Hornegger J 2012 *Nuclear Science Symposium and Medical Imaging Conference (NSS/MIC)*, October 27–November 3, 2012 California, USA, p. 2415

[19] Dennerlein F and Maier A 2012 *Medical Imaging* 2012*: Physics of Medical Imaing*, Februray 4–9, 2012 California, USA, p. 83131B

[20] Xia Y, Maier A and Hofmann H G 2013 *Medical Imaging* 2013*: Physics of Medical Imaging*, Februray 9–14, 2013 Florida, USA, p. 86681C

[21] Wang X C, Yan B, Li L and Hu G E 2012 *Chin. Phys. B* **21** 118702

[22] Toft P 1996 *The Radon Transform, Theory and Implementation* (Ph.D. Dissertation) (Copenhagen: Technical University of Denmark)